


Annealing optimization of graphitized $\text{Co}_3\text{O}_4@\text{CuO}@\text{NiO}$ composite electrodes for supercapacitor applications

Raphael M. Obodo^{1,2,3,4}  | Sylvester M. Mbam² | David C. Iwueke⁵ |
Muhammed Ramzan⁶ | Rufus Ijeh⁷ | Ishaq Ahmad^{3,4,8} | Maalik Maaza^{8,9} |
Fabian I. Ezema^{2,8,9,10}

¹Department of Physics, University of Agriculture and Environmental Sciences, Owerri, Imo State, Nigeria

²Department of Physics and Astronomy, University of Nigeria, Nsukka, Nigeria

³National Center for Physics, Quaid-i-Azam University, Islamabad, Pakistan

⁴NPU-NCP Joint International Research Center on Advanced Nanomaterials and Defects Engineering, Northwestern Polytechnical University, Xi'an, China

⁵Department of Physics, Federal University of Technology, Owerri, Imo State, Nigeria

⁶Department of Physics, Allama Iqbal Open University, Islamabad, Pakistan

⁷Department of Physics, University of Delta, Agbor, Nigeria

⁸Nanosciences African Network (NANOAFNET) iThemba LABS-National Research Foundation, Somerset West, Western Cape, South Africa

⁹UNESCO-UNISA Africa Chair in Nanosciences/Nanotechnology, College of Graduate Studies, University of South Africa (UNISA), Pretoria, South Africa

¹⁰Africa Centre of Excellence for Sustainable Power and Energy Development (ACE-SPED), University of Nigeria, Nsukka, Nigeria

Correspondence

Raphael M. Obodo, NPU-NCP Joint International Research Center on Advanced Nanomaterials and Defects Engineering, Northwestern Polytechnical University, Xi'an 710072, China.
Email: raphael.obodo@unn.edu.ng

Funding information

COMSATS Institute of Information Technology; National Center for Physics; Tertiary Education Trust Fund

Abstract

In recent times, carbon-based material has received a keen interest in the fabrication of electrodes because it enhances the performance of energy storage devices. Amalgamated composites of three transition metals ($\text{Co}_3\text{O}_4@\text{CuO}@\text{NiO}$) and graphene oxide (GO) were fabricated employing the hydrothermal method. The performance of some fabricated electrodes was optimized by annealing using various temperatures, examined for supercapacitor application using a three-electrode system. Our results indicate that $\text{Co}_3\text{O}_4@\text{CuO}@\text{NiO}$ -amalgamated electrode optimized using 100°C temperature shows enhanced features compared to deposited and other samples annealed at various temperatures. These discoveries also showed that $\text{Co}_3\text{O}_4@\text{CuO}@\text{NiO}$ -amalgamated electrode optimized using 100°C temperature delivered a specific capacitance of 1312 F/g from cyclic voltammetry analysis using 10.0 mV/s scan rate and 1258 F/g from galvanostatic charge-discharge analysis using 1.0 A/g current density. The cycling stability of electrodes annealed at 100°C was 92.5% after 10 000 cycles, indicating that annealing at 100°C enriched electrode characteristics.

KEYWORDS

annealing, electrode, graphene oxide, hydrothermal, supercapacitor

1 | INTRODUCTION

Recently, research on electrochemical energy storage devices has been of higher attention; this can be linked to the higher demands for environmental-friendly energy options, technological advancements, and the more demands for wireless electrical systems.

Supercapacitors possess highly fascinating properties such as greater power density, high durability, and exceptional performance when compared with the conventional electrochemical storage systems (like batteries and traditional capacitors).¹⁻³ Thus, supercapacitors have bridged the gap among the small energy density capacitors and the small power density batteries.⁴⁻⁷ Nevertheless, recent research has focused on improving the specific capacitance as well as the energy/power density of supercapacitors. Electrochemical double-layer capacitance (EDLC) and pseudocapacitance are the basic storage mechanisms associated with the majority of today's practical supercapacitors.⁸ EDLC mechanism involves an accretion of two opposite charges over the electrode-electrolyte edges, thus inducing a double layer effect. This primarily requires a counter migration of excess electrolyte ions to balance the insufficient conduction band electrons within near-surface area of the electrode/electrolyte boundary. EDLC mechanism is associated with carbon electroactive materials (such as graphene, carbon black, activated carbon, carbon aerogels, and carbon nanotubes).^{9,10} These carbon materials have enough surface area, excellent conductivity, and stability. However, supercapacitors made of carbon materials lack a remarkable energy density and specific capacitance.^{11,12} The pseudocapacitive mechanism arises from the effect of a quick and reversible charge migration across the electrode-electrolyte layer caused by a faradaic process.¹³⁻¹⁵ Unlike batteries, which also have a similar charge storage behavior, the pseudocapacitance in supercapacitors is a relay of the degree of charge reception and voltage fluctuation.^{16,17} Nowadays, metal oxide and conducting polymer are used as the main sources of electrode materials that exhibit the pseudocapacitance effect.^{18,19} Pseudocapacitors possess significant energy density and specific capacitance arising from a redox effect, compared to the electrochemical double-layer capacitors. Low-power density is, however, a major drawback of pseudocapacitors.^{20,21}

Electrodes comprising a mixture of carbon material and metal oxides have been widely reported to achieve improved electrochemical presentation. This denotes optimal synergistic influence between highly conductive carbon derivatives and redox-active metal oxides.^{22,23} Among the transition metal oxides, Co_3O_4 , CuO , and

NiO are among the recently researched electrode materials for applications in high-performance supercapacitors; this is because of their facile synthesis method, non-toxic nature, and remarkable theoretical capacitance.²⁴⁻²⁶

A hierarchical composite of $\text{NiO-Co}_3\text{O}_4\text{-NiO}$ with a fish thorns-like morphology ($\text{NiO NSAs@Co}_3\text{O}_4\text{-NiO FTNs}$) was synthesized through a chemical method for application in supercapacitors. This material offered a good areal capacity of up to $313 \mu\text{Ah}/\text{cm}^2$ using a current density of $4.0 \text{ mA}/\text{cm}^2$ and KOH electrolyte. The hierarchical composite was observed to exhibit an enhanced electrochemical behavior when compared to their lone pairs ($\text{Co}_3\text{O}_4\text{-NiO FTNs}$ and NiO NSAs). These improved features were credited to huge and porous surface area of the hierarchical composite electrode, coupled with a significant interaction among the mixed metal oxides.²⁷ Kim et al.²⁸ synthesized the composite of $\text{CuO}/\text{Co}_3\text{O}_4$ through a hydrothermal approach for application in supercapacitors. The electrode offered a high specific capacitance of up to $806.25 \text{ F}/\text{g}$ in a current density of $2 \text{ A}/\text{g}$, and 99.75% capacitance retention after 2000 cycles, which are of less value to that of the Co_3O_4 electrode. The composite electrode also exhibited a remarkable performance even under bending positions, which affords a promising material for flexible energy storage devices. A composite electrode comprising of an equal ratio of Co and Ni yielded a high specific capacitance of up to $1832 \text{ F}/\text{g}$ in $2.0 \text{ mA}/\text{cm}$ current density and KOH electrolyte. The electrode also retained up to 98% capacitance after 1000 charging and discharging cycles.²⁹ A hybrid structure comprising $\text{NiO@Co}_3\text{O}_4\text{@GQDs}$ for applications in lithium-ion batteries and supercapacitors was synthesized by Yini et al.³⁰ using a solvothermal technique. When used as a cathode in a supercapacitor, the composite electrode offered an improved specific capacitance value of up to $1361 \text{ F}/\text{g}$ under a current density of $1 \text{ A}/\text{g}$, while 76.4% capacitance was retained after 3000 cycling test. The exceptional performance of this hybrid electrode is credited to the multiple redox sites, enhanced conductivity, and improved ion diffusion, which are facilitated by the graphene material that also acted as a conductive support to $\text{NiO@Co}_3\text{O}_4$. An optimal synergistic effect between the metal oxides (NiO and Co_3O_4) and the graphene quantum dots majorly contributed to the increased electrochemical performance of the electrode when compared to single metal oxide.^{31,32} Our previous studies have also recorded an improved electrochemical behavior of mixed metal oxides when combined with graphene.³³⁻³⁵

The effect of calcination temperature on electroactive material was reported by Shaikh et al.³⁶ and Jadhav et al.³⁷ It was observed that both the redox capability and

electrochemical stability of the electrode increased significantly with the annealing temperature. This is due to the optimized oxidation and reduced particle boundary density caused by the higher temperature.

In this work, we, hereby, present studies, findings, and performance of annealing optimization of graphitized hierarchical $\text{Co}_3\text{O}_4@\text{CuO}@\text{NiO}$ for fabricated electrodes for supercapacitor applications. Our work employed in the enhancement of $\text{Co}_3\text{O}_4@\text{CuO}@\text{NiO}$ electrodes by increasing surface area, rate capability, reaction kinetics, providing sufficient electroactive spots, multiple ion transport pathways, superior charge collection ability and rapid redox reaction kinetics occasioned by the addition of graphene oxide (GO), and increasing redox capability and electrochemical stability due to increased annealing optimization of $\text{Co}_3\text{O}_4@\text{CuO}@\text{NiO}$ electrodes.

2 | EXPERIMENTAL SECTION

2.1 | Materials

Modified Hummers technique was employed in the synthesis of graphene oxide. Other chemicals and reagents used were obtained from Sigma-Aldrich. The entire reagents used were of analytical grade.

2.2 | Synthesis techniques

About 50.0 ml, 0.5 M each of $\text{CoCl}_2 \cdot 6\text{H}_2\text{O}$, $\text{Cu}(\text{NO}_3)_2 \cdot 6\text{H}_2\text{O}$, and $\text{Ni}(\text{NO}_3)_2 \cdot 6\text{H}_2\text{O}$ solutions was formed separately. Various salt solutions were mixed together in a beaker and 0.01 g of GO was produced using modified Hummer's technique and dissolved in 20 ml of distilled water and was transferred inside the mixed solution. All the mixed solutions were stirred for 30 min for homogeneity. A neutral solution was needed; therefore, 1.0-M sodium hydroxide (NaOH) solution was added dropwise, while stirring with a magnetic stirrer was continued for another 30 min until a solution with pH 7 was obtained. This stirred, homogenous, and neutral solution was dispensed inside a 300-ml autoclave and four 2 by 2 cm^2 pieces of fluorine-doped tin oxide glass substrates were fixed in the autoclave using Teflon tape and rod. This autoclave was placed into an oven and heated to 180°C for 7 h. In the end, a thin film of composite material was formed on the glass substrates, removed, and rinsed using distilled water and was used for various analyses. The synthesis process employed in the course of the experimentation is shown in Figure 1.

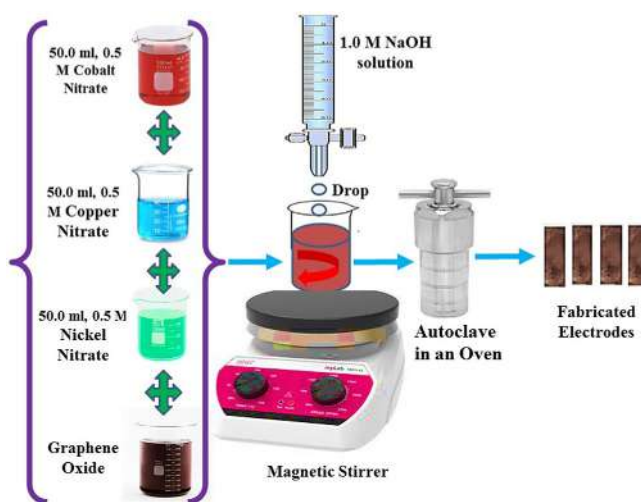


FIGURE 1 Synthesis procedure used in fabricating electrodes

2.3 | Characterizations

The crystal configurations, morphologies, and compositions of electrodes were examined using X-ray diffraction (XRD), scanning electron microscopy (SEM), and energy-dispersive X-ray (EDS), respectively. The XRD patterns of various electrodes were measured on a Shimadzu XRD-6000 X-ray diffractometer with a range of $2\theta = 10^\circ\text{--}60^\circ$ using $\text{Cu K}\alpha$ radiations ($k = 0.154178 \text{ nm}$) and high-resolution SEM operating with EDS, respectively. The functional groups present in the pristine electrode were examined using Fourier transform infrared (FTIR). The UV-visible spectrophotometer was used in assessing the absorption properties of various electrodes amid 350–1100 nm range of wavelength.

2.4 | Electrochemical analysis

Cyclic voltammetry (CV), galvanostatic charge-discharge (GCD), and electrochemical impedance spectroscopy (EIS) examinations of various electrodes were tested with Gamry potentiostat using 1.0-M Na_2SO_4 aqueous electrolyte under the three-electrode arrangement. We maintained the tested area of electrodes at 1.5 by 1.5 cm^2 . Saturated Ag/AgCl and graphite rod were employed as the reference and counter electrodes correspondingly. EIS assessment was executed using frequency ranges of 1.0–100.0 kHz. Pristine electrodes stability test was conducted using a current density of 1.0 A/g over 10 000 cycles employing a three-electrode scheme.

3 | RESULTS AND DISCUSSIONS

3.1 | Phase analysis

The powder XRD machine was employed to study the phase and crystallographic properties of various samples and X'pert high score was used for the analysis. Figure 2 presents the XRD spectra of graphitized $\text{Co}_3\text{O}_4@\text{CuO}@\text{NiO}$ annealed at different temperatures. These spectra consist of orthorhombic phases of cobalt copper oxide (CoCu_2O_3) with JPCDS No. 00-021-0288 and tetragonal copper nickel oxide (CuNiO_2) with JPCDS No. 00-006-0720. The 2θ peak positions of CoCu_2O_3 appear at 29.70° , 33.00° , 36.71° , 39.29° , and 48.38° with corresponding reflections of (011), (012), (103), (004), and (014), respectively. CuNiO_2 possesses 2θ angle peak positions at 36.71° and 42.50° with reflection planes of (111) and (200), respectively. The peaks of GO and rGO appeared at 2θ angle approximately equal to 10.85° and 25.01° in the pristine and 100°C annealed samples, respectively. However, for samples annealed at 200 and 300°C , the peak of GO disappeared, while the peak of rGO remains, but there is a reduction in rGO peak intensity as annealing temperature increases. Various samples possess a common peak at 2θ angle equal to 36.71° confirming a synergistic collaboration among various transition metal oxides in the composite. The pristine and annealed samples are closely indexed to the standard pattern of their pure oxides without any impurities. Sharp peaks observed in all the XRD spectra confirm the formation of high crystalline Co_3O_4 , CuO, and NiO samples, and these sharp peaks are reduced as annealing temperature increases. Crystallite sizes of various nanomaterials were estimated using the Scherrer equation as shown in Equation (1).³⁸

$$D = \frac{0.9\lambda}{\beta \cos\theta} \quad (1)$$

where D stands for crystallite size, λ represents incident radiation wavelength ($\lambda = 1.5406 \text{ \AA}$), β is the peak width

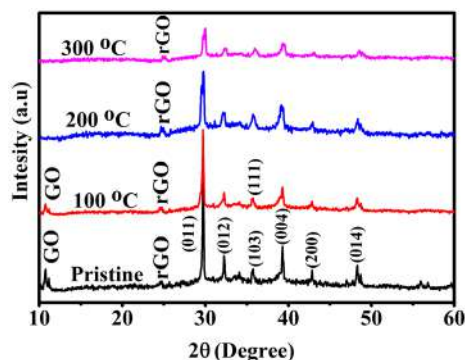


FIGURE 2 XRD spectra of pristine and annealed electrodes. XRD, X-ray diffraction

TABLE 1 Summary of electrodes and crystallite sizes

S/N	Electrodes	Crystallite sizes (nm)
1.	Pristine	36.58
2.	Annealed at 100°C	32.44
3.	Annealed at 200°C	28.22
4.	Annealed at 300°C	24.78

at its half maximum compared with 2θ , and θ is diffraction angle. Table 1 shows the summary of electrodes and crystallite sizes.

3.2 | Morphology studies

Scanning electron microscopy equipment was engaged for more understanding of the morphology of the fabricated electrode as shown in Figure 3A–D. SEM images present spherical and platelets of randomly adhered particles covering the whole substrate surface with some accumulations to form constellations of particles at some points. The presence of some white patches at some points on the surface of various substrates indicates the presence of GO, which enhances the uniformity and elemental anchoring on the skeleton of GO, demonstrating that GO has an indispensable influence on the crystal growth of these electrodes.³⁰ Figure 3A shows the SEM of pristine $\text{Co}_3\text{O}_4@\text{CuO}@\text{NiO}$ electrode; it indicates the presence of spherical, platelet, and few rod-like structures with bigger grains of particles compared to annealed electrodes. Figure 3B presents SEM image of graphitized hierarchical $\text{Co}_3\text{O}_4@\text{CuO}@\text{NiO}$ sample electrode annealed using the temperature of 100°C , the platelets and rods observed in the pristine electrodes disappeared, and only spherical particles persisted with few agglomerations. Figure 3C reveals the SEM image of graphitized ranked $\text{Co}_3\text{O}_4@\text{CuO}@\text{NiO}$ electrode annealed at 200°C ; the size of the spherical particles reduced, while the number of particles and agglomerations increased. Figure 3D discloses the SEM image of $\text{Co}_3\text{O}_4@\text{CuO}@\text{NiO}$ electrode annealed at 300°C ; there is a drastic reduction in spherical particle size and increased formation of aggregates of particle indicating movement to amorphization of the electrode. However, electrodes' porous nature assisted various ions' migration and integration, which means, enhancing the electrochemical performance of various electrodes, especially for electrodes annealed at 100°C .

3.3 | Elemental compositional analysis

The equivalent EDS pattern of pristine graphitized hierarchical $\text{Co}_3\text{O}_4@\text{CuO}@\text{NiO}$ electrode is shown in

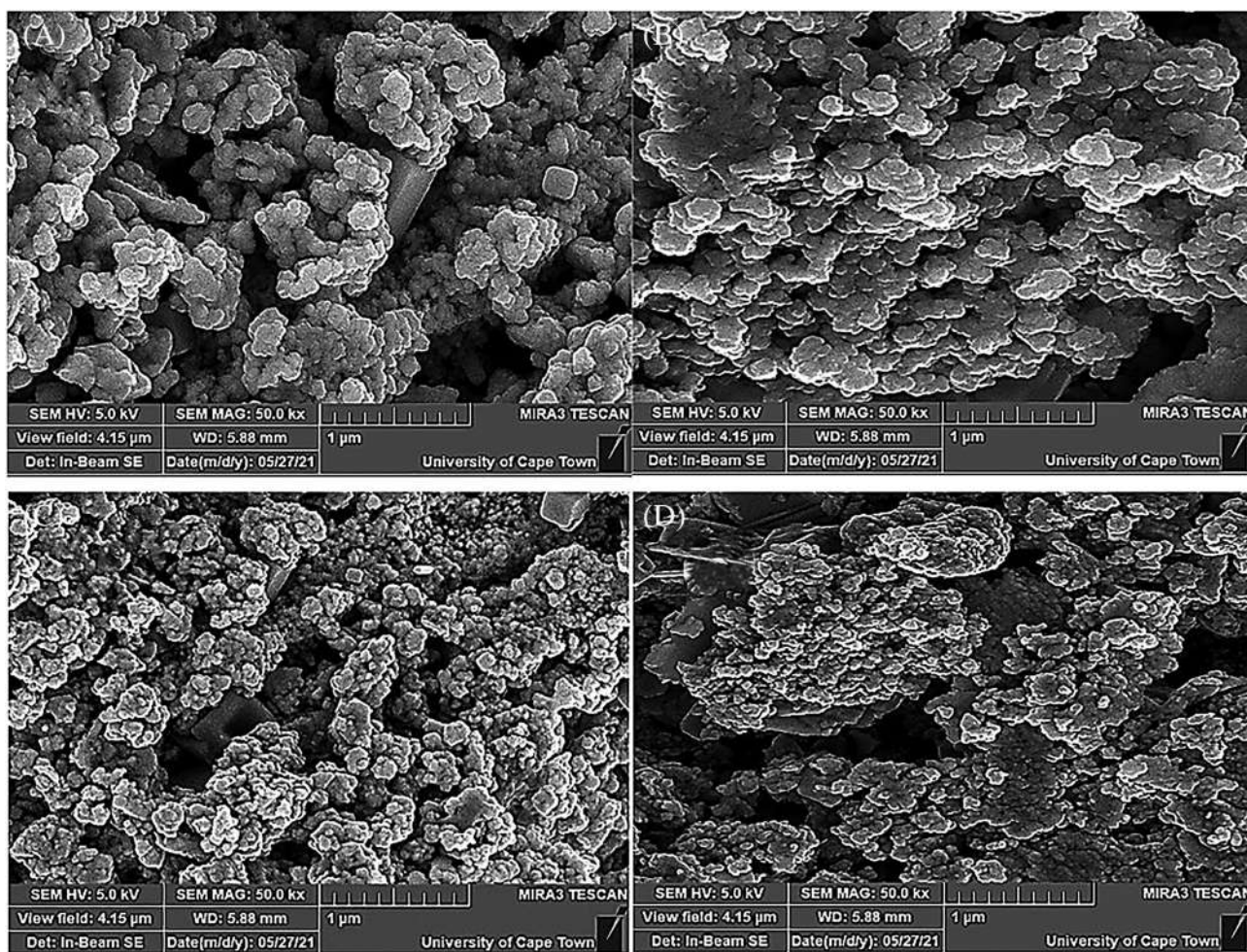


FIGURE 3 SEM micrographs of $\text{Co}_3\text{O}_4@\text{CuO}@\text{NiO}$ electrodes (A) pristine, annealed at (B) 100°C (C) 200°C (D) 300°C . SEM, scanning electron microscopy

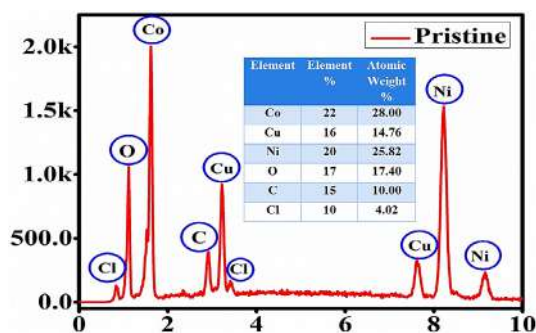


FIGURE 4 EDS spectrum of $\text{Co}_3\text{O}_4@\text{CuO}@\text{NiO}$ electrode. EDS, energy-dispersive X-ray

Figure 4. The spectrum obtained confirmed that the fabricated pristine electrode has Co, Cu, Ni, O, C, and Cl element peaks alone without impurities in the fabricated electrode. It also confirms that the electrode was synthesized without impurities, showing corresponding metal ions used, while the outstanding manifestation of oxygen

peak with prominent intensity indicates that the electrode was efficiently fabricated and each metal ion transformed to their respective metal oxides.⁶ The presence of carbon (C) element peak in the EDS spectrum confirmed the presence of reduced graphene oxide, a derivative of carbon. The presence of chlorine is also observed in the EDS spectrum; this chlorine emanated from hydrogen chloride acid (HCl) used during the synthesis of reduced graphene oxide, which formed a part of GO functional groups.

3.4 | Functional groups analysis

Figure 5 displays the FTIR spectroscopy showing the molecular sensations of various functional groups existing and contained by the 500 cm^{-1} – 4000 cm^{-1} wavelength ranges. The obvious hollow in the spectrum of the pristine electrode around 3420 and 1450 cm^{-1} occurred because of stretching and vibrations of water molecules.²⁶

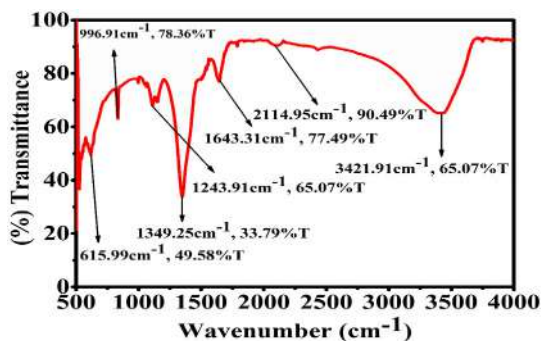


FIGURE 5 FTIR spectrum of pristine $\text{Co}_3\text{O}_4@\text{CuO}@\text{NiO}$ electrode. FTIR, Fourier transform infrared

TABLE 2 Analysis of functional groups in pristine and graphitized $\text{Co}_3\text{O}_4@\text{CuO}@\text{NiO}$ electrode

S/N	Wavenumber ranges	Functional groups
1.	3550–3200	Hydroxyl compound
2.	1432–1621	Aromatic ring
3.	1150–911	C–O–C group
4.	858–733	C–H

Various functional groups captivate sun energy at a given specific frequency, which matches with given vibrations including epoxy, hydroxyl, carboxylic, aromatic, and carbonyl.^{39,40} Various chemicals utilized in GO synthesis and metal oxide vibrations all contributed to these functional groups present in the pristine electrode. Table 2 is the breakdown of functional groups in pristine and graphitized $\text{Co}_3\text{O}_4@\text{CuO}@\text{NiO}$ electrode.

3.5 | Optical analysis

Light absorption features of graphitized hierarchical $\text{Co}_3\text{O}_4@\text{CuO}@\text{NiO}$ electrodes were analyzed with the help of a UV–visible spectrophotometer using a wavelength range of 350–1100 nm. Figure 6A shows the schemes of optical wavelength against absorbances of various electrodes. The electrode absorbance fell from the visible part of the electromagnetic spectrum and advanced by diminishing, while wavelength increased in the direction of the near-infrared region, as observed in all electrodes. The results of electrode absorbance show low absorbance properties for pristine and electrode annealed at 100°C, but high absorbance for electrodes annealed at 200 and 300°C. Low absorbance recorded in pristine and electrode annealed at 100°C may be attributed to the presence of GO in the electrode. However, when the temperature rises, the absorbance of electrodes annealed at 200 and 300°C rises, which could be due to

GO to rGO conversion. Tauc's equation was used to calculate the optical bandgaps of these electrodes, as presented in Equation (2).

$$\alpha = A(h\nu - E_g)^n \quad (2)$$

However, in a straight bandgap transition, α is the absorption coefficient, E_g is the absorption bandgap, and A is a constant and n is $\frac{1}{2}$.

The assessed bandgap energies for pristine graphitized $\text{Co}_3\text{O}_4@\text{CuO}@\text{NiO}$ and annealed at 100, 200, and 300°C electrodes are 2.00, 1.90, 2.47, and 2.52 eV correspondingly. Extrapolating the undeviating portion of each plot of $(ah\nu)^2$ against $(h\nu)$ axis yielded various bandgap energy values for each electrode. The synergistic alliance among transition metal oxides GO⁴¹ produced a reduced bandgap energy suitable for applications in an energy storage device.

3.6 | Electrochemical studies

The redox nature of various electrodes was examined using CV plots shown in Figure 7A–D. Scan speeds of 10, 20, 30, 40, 50, 70, 80, 90, and 100 mV/s with a voltage window of 0.0–0.7 V were used to record various curves of fabricated electrodes. The appearance of faradic reversible redox peaks prompted by surface adsorption of ions between electrodes and electrolyte explains the double-layer capacitance storage mechanism of fabricated electrodes.⁴² The nonexistence of shape distortion in CV curves in all scan rates demonstrated the redox stability of the fabricated electrodes.⁴² The large integrated area of CV loops indicates that these electrodes are good double-layer capacitive electrodes.^{43,44}

Equation (3)⁴⁵ was used to estimate the specific capacitance value of various electrodes produced using CV curves.

$$C_{\text{sp}} = \frac{1}{mVs} \int i(V)dV (F/g) \quad (3)$$

where m is the mass loaded in mg, V is the potential window used in volts, S is the sweep rate in mV/s, and i is the current applied in ampere (A).

The calculated specific capacitance of various fabricated electrodes using 10.0 mV/s scan rate, which is the scan rate with the highest specific capacitance, is 1146, 1312, 875, and 772 F/g for pristine, annealed at 100, 200, and 300°C, respectively. These results indicate that moderate annealing enhances the performance of synthesized electrodes.

FIGURE 6 Plots of (A) absorbance and (B) energy bandgap values of pristine and annealed $\text{Co}_3\text{O}_4@/\text{CuO}@/\text{NiO}$ electrodes

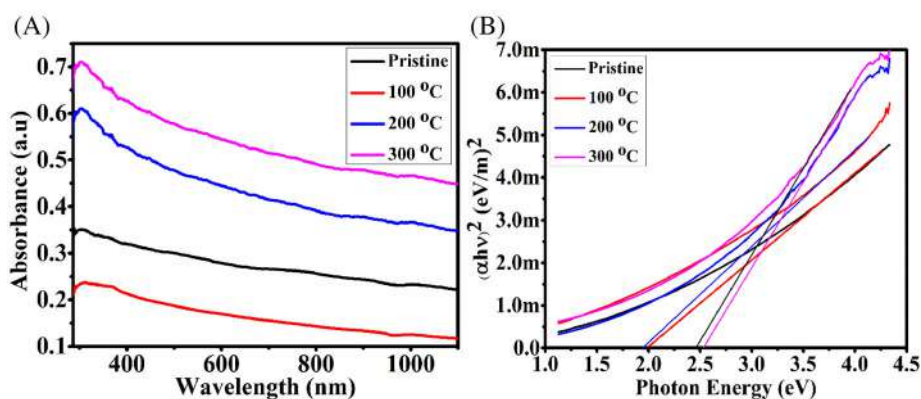
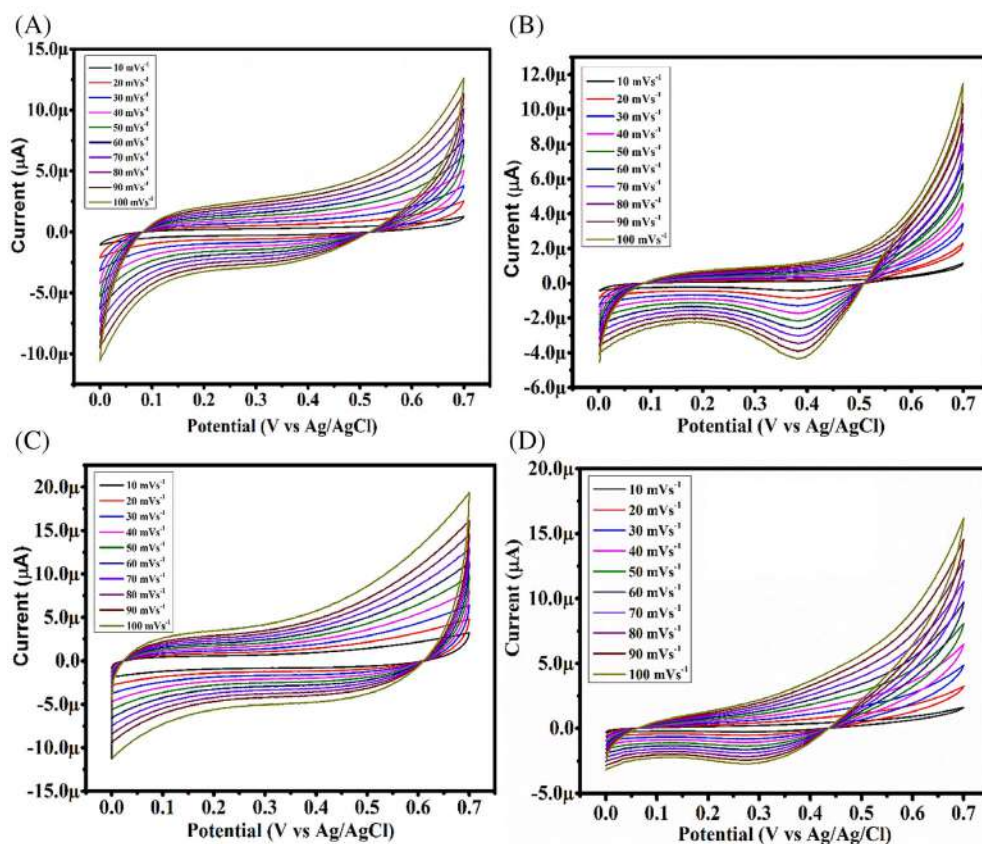


FIGURE 7 CV plots of (A) pristine, annealed at (B) 100 °C, (C) 200 °C, and (D) 300 °C electrodes. CV, cyclic voltammetry



We measured electrodes' specific capacitance, energy, and power densities using GCD with 1.0 A/g current density, as shown in Figure 8A. The electrolytic conditions employed in the GCD investigation were the same as those used in the CV measurements. Equation (4)⁴³ was used to compute the specific capacitance.

$$C_s = \frac{I}{m \frac{dV}{dt}} (F/g) \quad (4)$$

where dV/dt denotes GCD's slope, m denotes active mass loaded, and I stands for current employed throughout the test. The computed specific capacitances from Figure 8A

show that pristine, annealed at 100, 200, and 300 °C, respectively, achieved 1022, 1258, 945, and 715 F/g. Results obtained show that sample electrode annealed using 100 °C performed better matched with other fabricated electrodes. This bizarre behavior could be attributed to recrystallization that occurred after the annealing temperature provided heat energy.² The energy (E_d) and power (P_d) densities were calculated using Equations (5) and (6).¹⁴

$$E_d = 0.5C_s(\Delta V)^2 \quad (5)$$

$$P_d = 3.6 \frac{E_d}{t} \quad (6)$$

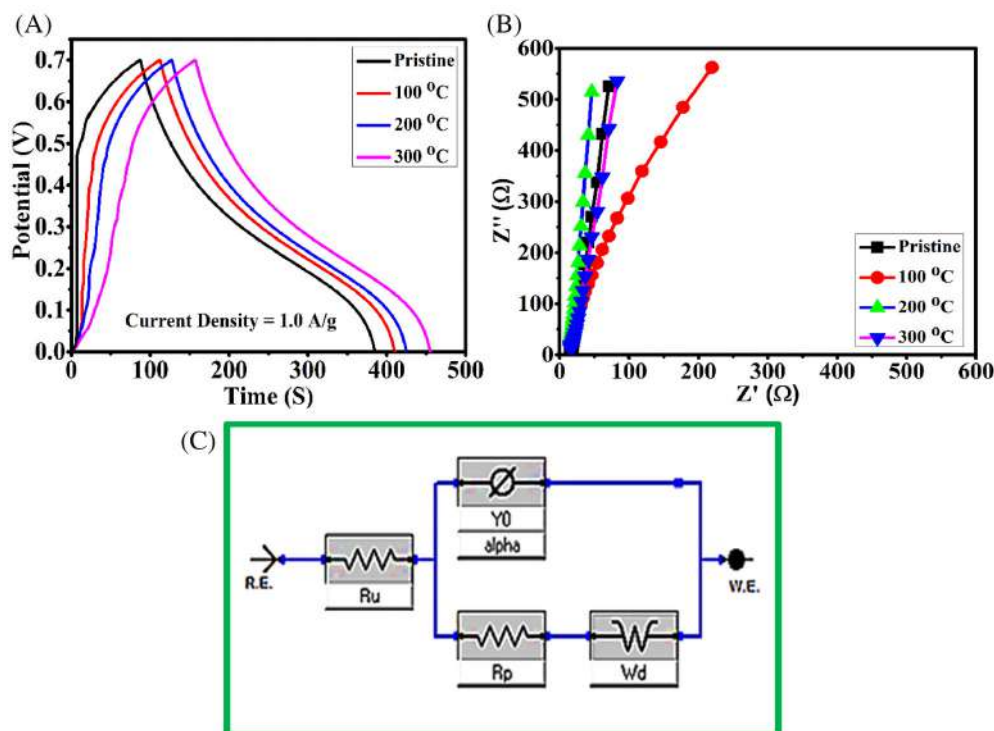


FIGURE 8 (A) GCD and (B) EIS plots of various electrodes (C) CPE with the diffusion model. CPE, constant phase element; EIS, electrochemical impedance spectroscopy; GCD, galvanostatic charge–discharge

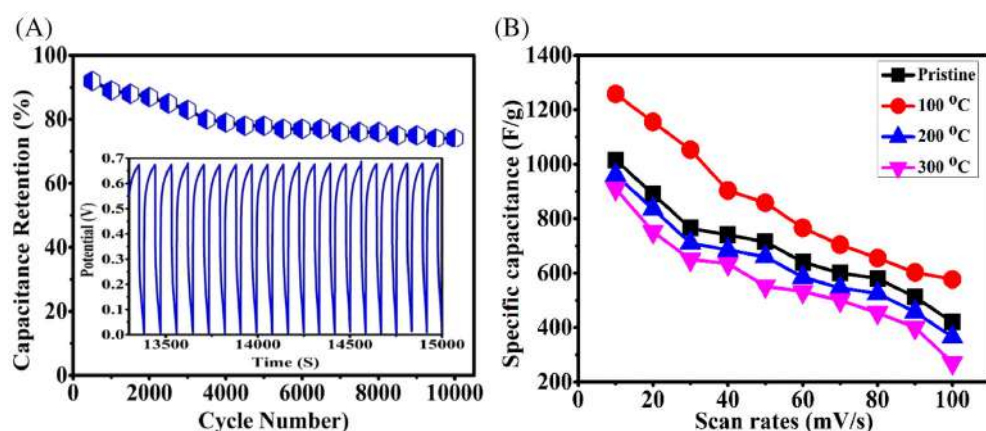


FIGURE 9 Plots of (A) Specific capacitance versus scan rates of various electrodes and (B) stability test of electrode annealed at 100°C

where ΔV stands for potential window used and t represents the time to discharge. The calculated energy densities from Figure 8A were 250.39, 308.21, 231.21, and 175.18 Wh/Kg, respectively, for pristine, annealed at 100, 200, and 300°C with respective power densities of 4.55, 5.69, 4.21, and 3.20 W/Kg.

The electrochemical system's reaction kinetics was studied using EIS. As shown in Figure 8B, the EIS was performed at room temperature with a frequency range of 1.0 Hz–100.0 kHz. In the EIS investigation, the equivalent electrical circuit model of the constant phase element (CPE) was adopted. Using the Nyquist plot, CPE with the diffusion model in Figure 8C was used in calculating the resistance fitted with a Nyquist plot. The model was utilized to evaluate the resistance of electrolytic

solution and produced electrodes, and it matched absolutely. Various electrodes have electrolytic resistances (R_e) of 3.0, 1.5, 8.0, and 12.0 for pristine, annealed at 100, 200, and 300°C, and working electrode resistances (R_w) of 0.05, 0.02, 0.09, and 1.08 for pristine, annealed at 100, 200, and 300°C, respectively.

The cycle stability and efficiency of graphitized $\text{Co}_3\text{O}_4@\text{CuO}@\text{NiO}$ sample electrode annealed using a temperature of 100°C having a superior property were tested using a current density of 1.0 A/g for continuous 10 000 cycles as illustrated in Figure 9A. The result of the cycling test obtained from the electrode annealed at 100°C, which delivered a healthier performance, also displayed advanced cycle stability of 92.5% after delivering 10 000 cycles displaying that optimization by annealing

using the temperature of 100°C enhanced electrodes' performance. GCD plots of the ending 20 cycles were shown as an inset in Figure 9A, varied marginally, indicating good cyclic stability.³⁸ The coulombic efficiency of graphitized Co₃O₄@CuO@NiO fabricated electrode and optimized with 100°C temperature was assessed by means of the formula presented in Equation (7). The coulombic efficiency (η) defines the efficiency as well as rate of charge transmission within arrangement or scheme, which was used in rating electrochemical reactions.

$$\eta = \frac{T_d}{T_c} \times 100\% \quad (7)$$

where T_d and T_c signify the time to discharge and charge correspondingly. The coulombic efficiency of the electrode annealed at 100°C was estimated to be 92.5%. Figure 9B presents the specific capacitance vs scan rates as obtained from the CV of various graphitized Co₃O₄@CuO@NiO electrodes. The study showed that the specific capacitance of various electrodes changed marginally, confirming an excellent cyclic reversibility.

4 | CONCLUSIONS

Graphitized hierarchical Co₃O₄@CuO@NiO electrodes were admirably invented by means of the hydrothermal technique for use in supercapacitor electrodes. GO was incorporated in the nanostructured electrodes synthesized because of its pronounced surface area and high electrical conductivity. The mutual collaboration between the transition metal mixtures and GO enhanced electrodes features life span and firmness. Results obviously indicate that the addition of GO as well as moderate annealing enhanced the performance of the electrode; however, restrained annealing is required because annealing at higher temperature reduced electrodes' performance. The interaction between graphene oxide and composite metal ions enhanced the performance of Co₃O₄@CuO@NiO electrodes. It is also observed that moderate annealing increased redox capability and electrochemical stability, hence, increasing Co₃O₄@CuO@NiO electrodes' performance. The coulombic efficiency of the electrode annealed at 100°C is 92.5%, better than pristine and annealed at higher temperatures, confirming that annealing at a moderate temperature optimized the performance of the electrode.

ACKNOWLEDGMENTS

RMO and IA humbly acknowledge NCP for their PhD fellowship (NCP-CAAD/PhD-132/EPD) award and

COMSATS for the travel grant for the fellowship. FIE graciously acknowledges the grant by TETFUND under contract number TETFUND/DR&D/CE/UNI/NSUKKA/RP/VOL.I and also acknowledge the support received from the Africa Centre of Excellence for Sustainable Power and Energy Development (ACE-SPED), University of Nigeria, Nsukka, that enabled the timely completion of this research. We thank Engr. Emeka Okwuosa for the generous sponsorship of April 2014, July 2016, July 2018, and July 2021 conferences/workshops on applications of nanotechnology to energy, health, and environment and for providing some research facilities.

CONFLICT OF INTEREST

The authors have no conflict of interest to disclose.

DATA AVAILABILITY STATEMENT

The authors confirm that the data supporting the findings of this study are available from the corresponding author [Dr. R. M. Obodo] upon reasonable request.

ORCID

Raphael M. Obodo  <https://orcid.org/0000-0001-7418-8526>

REFERENCES

1. Aneke M, Wang M. Energy storage technologies and real life applications: a state of the art review. *Appl Energy*. 2016;179:350-377.
2. Conway BE. Transition from 'Supercapacitor' to 'Battery' behavior in electrochemical energy storage. *J Electrochem Soc*. 1999;138(6):1539-1548.
3. Kim BJ, Sy S, Yu A, Zhang J. *Electrochemical Supercapacitors for Energy Storage and Conversion*. Hoboken, NJ: John Wiley & Sons Ltd; 2015.
4. Simon P, Gogotsi Y, Dunn B. Where do batteries end and supercapacitors begin. *Science*. 2014;343(6176):1210-1211.
5. Pawar SA, Patil DS, Shin JC. Transition of hexagonal to square sheets of Co₃O₄ in a triple heterostructure of Co₃O₄/MnO₂/GO for high performance supercapacitor electrode. *Curr Appl Phys*. 2019;19:794-803.
6. Zhu D, Shao Y. NiO/ZnO nanocomposite as electrode material for supercapacitors. *Int J Electrochem Sci*. 2018;13:3601-3612.
7. Zhu Y, Peng L, Chen D, Yu G. Intercalation pseudocapacitance in ultrathin VOPO₄ nanosheets: toward high-rate alkali-ion-based electrochemical energy storage. *Nano Lett*. 2016;61:742-747.
8. Xin L, Bingqing W. Supercapacitors based on nanostructured carbon. *Nano Energy*. 2013;2:159-173.
9. Ratajczak P, Suss ME, Kaasik F, Béguin F. Carbon electrodes for capacitive technologies. *Energy Storage Mater*. 2019;16:126-145.
10. Parida K, Bhavanasi V, Kumar V, Wang J, Lee PS. Fast charging self-powered electric double layer capacitor. *J Power*. 2017;342:70-78.

11. Jian X, Liu S, Gao Y, et al. Carbon-based electrode materials for supercapacitor: progress, challenges and prospective solutions. *Journal of Electrical Engineering*. 2016;4:75-87.
12. Obodo RM, Ahmad I, Ezema FI. Introductory chapter: graphene and its applications. In: Ahmad I, Ezema FI, eds. *Graphene and its Derivatives-Synthesis and Applications*. London, UK: IntechOpen; 2019.
13. Brousseau T, Bélanger D, Long JW. To be or not to be pseudocapacitive. *J Electrochem Soc*. 2015;162(5):A5185-A5189.
14. Obodo RM, Chime U, Nkele AC, et al. Effect of annealing on hydrothermally deposited Co_3O_4 -ZnO thin films for supercapacitor applications. *Mater Today Proc*. 2021;36:374-378.
15. Obodo RM, Shinde NM, Chime UK, et al. Recent advances in metal oxide/hydroxide on three-dimensional nickel foam substrate for high performance pseudocapacitive electrodes. *Curr Opin Electrochem*. 2020;21:242-249.
16. Pilatowicz G, Budde-Meiwes H, Kowal J, et al. Determination of the lead-acid battery's dynamic response using Butler-Volmer equation for advanced battery management systems in automotive applications. *J Power Sources*. 2016;331:348-359.
17. Sharma RK, Ghose R. Synthesis of Co_3O_4 -ZnO mixed metal oxide nanoparticles by homogeneous precipitation method. *J Alloys Compd*. 2016;686:64-73.
18. Berrueta A, Ursua A, Martin IS, Eftekhari A, Sanchis P. Supercapacitors: electrical characteristics, modeling, applications, and future trends. *IEEE Access*. 2019;7:50869-50896.
19. Obodo RM, Sayyed SG, Mahadik MA, et al. Transition metal oxide-based nanomaterials for high energy and power density supercapacitor. *Electrochemical Devices for Energy Storage Applications*. United Kingdom: Taylor & Francis Group, CRC Press; 2019:131-150.
20. Jiang Y, Liu J. Definitions of pseudocapacitive materials: a brief review. *Energy Environ Mater*. 2019;2(1):30-37.
21. Nwanya AC, Ndipingwi MM, Ikpo CO, et al. *Zea mays* leaf extract mediated synthesis of nickel oxide nanoparticles as positive electrode material for asymmetric supercapacitor. *J Alloys Compd*. 2020;822:153581.
22. Muzaffar A, Ahamed MB, Deshmukh K, Thirumalai J. A review on recent advances in hybrid supercapacitors: design, fabrication and applications. *Renew Sustain Energy Rev*. 2019;101:123-145.
23. Sayyed SG, Mahadik MA, Shaikh AV, Jang SJ, Pathan HM. Nano-metal oxide based supercapacitor via electrochemical deposition. *ES Energy & Environment*. 2019;3(4):25-44.
24. Li Z, Zhang W, Liu Y, Guo J, Yang B. 2D nickel oxide nanosheets with highly porous structure for high performance capacitive energy storage. *J Phys D Appl Phys*. 2018;51(4):045302.
25. Yang S, Liu Y, Hao Y, et al. Oxygen-vacancy abundant ultrafine Co_3O_4 /graphene composites for high-rate supercapacitor electrodes. *Adv Sci*. 2018;5:1700659.
26. Singh AK, Sarkar D, Karmakar K, Mandal K, Khan GG. High-performance supercapacitor electrode based on cobalt oxide-manganese dioxide-nickel oxide ternary 1D hybrid nanotubes. *ACS Appl Mater Interfaces*. 2016;8(32):20786-20792.
27. Sekhar SC, Nagaraju G, Yu JS. High-performance pouch-type hybrid supercapacitor based on hierarchical $\text{NiO-Co}_3\text{O}_4$ - NiO composite nanoarchitectures as an advanced electrode material. *Nano Energy*. 2018;48:81-92.
28. Kim HJ, Kim SY, Lim LJ, Reddy AE, Gopi CVVM. Facile one-step synthesis of a composite $\text{CuO/Co}_3\text{O}_4$ electrode material on Ni foam for flexible supercapacitor applications. *New J Chem*. 2017;41(13):5493-5497.
29. Xu H, Zhuang J, Chen Y, Wu J, Zhang J. Preparation and performance of Co_3O_4 - NiO composite electrode material for supercapacitors. *RSC Adv*. 2014;4(30):15511-15517.
30. Yin X, Zhi C, Sun W, Lv LP, Wang Y. Multilayer $\text{NiO@Co}_3\text{O}_4$ @graphene quantum dots hollow spheres for high-performance lithium-ion batteries and supercapacitors. *J Mater Chem A*. 2019;7(13):7800-7814.
31. Niveditha CV, Aswini R, Jabeen Fatima MJ, Ramanarayan R, Pullanjiyot N, Swaminathan S. Feather like highly active Co_3O_4 electrode for supercapacitor application: a potentiodynamic approach. *Materials Research Express*. 2018;6:065501.
32. Ghalmi Y, Habelhames F, Sayah A, et al. Capacitance performance of NiO thin films synthesized by direct and pulse potentiostatic methods. *Ionics*. 2019;25(12):6025-6033.
33. Obodo RM, Nwanya AC, Ike IS, Ahmad I, Ezema FI. Role of carbon derivatives in enhancing metal oxide performances as electrodes for energy storage devices. In: Lonkade CD, Ezema FI, eds. *Chemically Deposited Nanocrystalline Metal Oxide Thin Films*. New York, NY: Springer; 2021:469-488.
34. Obodo RM, Nwanya AC, Ekwealor ABC, et al. Influence of pH and annealing on the optical and electrochemical properties of cobalt (III) oxide (Co_3O_4) thin films. *Surf Interfaces*. 2019;16:114-119.
35. Obodo RM, Ahmad A, Jain GH, Ahmad I, Maaza M, Ezema FI. 8.0 MeV copper ion (Cu^{++}) irradiation-induced effects on structural, electrical, optical and electrochemical properties of Co_3O_4 - NiO -ZnO/GO nanowires. *Materials Science for Energy Technologies*. 2020;3:193-200.
36. Shaikh JS, Pawar RC, Mali SS, Moholkar AV, Kim JH, Patil PS. Effect of annealing on the supercapacitor performance of CuO-PAA/CNT films. *J Solid State Electrochem*. 2012;16(1):25-33.
37. Jadhav VV, Kore RM, Thorat ND, et al. Annealing environment effects on the electrochemical behavior of supercapacitors using Ni foam current collectors. *Mater Res Express*. 2018;5(12):125004.
38. Obodo RM, Chibueze TC, Ahmad I, et al. Effects of copper ion irradiation on $\text{Cu}_y\text{Zn}_{1-2y-x}\text{Mn}_x/\text{GO}$ supercapacitive electrodes. *J Appl Electrochem*. 2021;51:829-845.
39. Sun M, Liu H, Liu Y, Qu J, Li J. Graphene-based transition metal oxide nanocomposites for the oxygen reduction reaction. *Nanoscale*. 2015;7:1250-1269.
40. Ando T, Ishii M, Kamo M, Sato Y. Faraday Trans. *J Chem Soc*. 1993;89:1783-1789.
41. Obodo RM, Ahmad I, Ezema FI. Introductory chapter: graphene and its applications. *Dermatol Int*. 2019;1:86023.
42. Arasi SE, Ranjithkumar R, Devendran P, Krishnakumar M, Arivarasan A. Studies on electrochemical mechanism of nanostructured cobalt vanadate electrode material for pseudocapacitors. *J Energy Storage*. 2021;41:102986.
43. Obodo RM, Onah EO, Nsude HE, et al. Performance evaluation of graphene oxide based Co_3O_4 @GO, MnO_2 @GO and $\text{Co}_3\text{O}_4/\text{MnO}_2$ @GO electrodes for supercapacitors. *Electroanalysis*. 2020;32:2786-2794.

44. Obodo RM, Asjad M, Nwanya AC, et al. Evaluation of 8.0 MeV carbon (C^{2+}) irradiation effects on hydrothermally synthesized $Co_3O_4/CuO/ZnO@GO$ electrodes for supercapacitor applications. *Electroanalysis*. 2020;32:2958-2968.
45. Mao X, Wang Y, Xiang C, et al. Core-shell structured $CuCo_2S_4@CoMoO_4$ nanorods for advanced electrode materials. *J Alloys Compd*. 2020;844:156133.

How to cite this article: Obodo RM, Mbam SM, Iwueke DC, et al. Annealing optimization of graphitized $Co_3O_4@CuO@NiO$ composite electrodes for supercapacitor applications. *Energy Storage*. 2022;e347. doi:[10.1002/est2.347](https://doi.org/10.1002/est2.347)